X-626-72-269
PREPRINT

NASA TM X- 65982

AN INVESTIGATION OF GEOMETRY AND NOISE CORRECTIONS TO SAN MARCO-C NEUTRAL ATMOSPHERIC COMPOSITION EXPERIMENT DATA
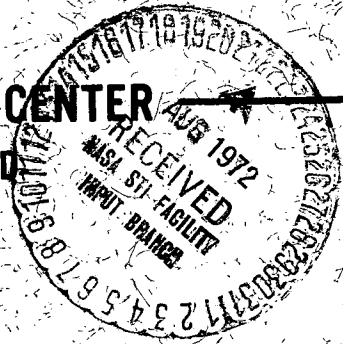
STEVEN A. CURTIS

JULY 1972

GSFC —— GODDARD SPACE FLIGHT CENTER
GREENBELT, MARYLAND

RECEIVED
NASA STI FACILITY
INPUT BRANCH

AN INVESTIGATION OF GEOMETRY AND NOISE CORRECTIONS

TO SAN MARCO-C NEUTRAL ATMOSPHERIC

COMPOSITION EXPERIMENT DATA

Steven A. Curtis
Data Analysis Branch
Laboratory for Planetary Atmospheres
Greenbelt, Maryland

July 1972

GODDARD SPACE FLIGHT CENTER
Greenbelt, Maryland

AN INVESTIGATION OF GEOMETRY AND NOISE CORRECTIONS TO SAN MARCO-C NEUTRAL ATMOSPHERIC COMPOSITION EXPERIMENT DATA

Steven A. Curtis
Data Analysis Branch
Laboratory for Planetary Atmospheres
Greenbelt, Maryland

ABSTRACT

The problem of the calculation of ambient densities from SM-C NACE data is considered. A brief description is given of the data measurement method, followed by a description of both the theoretical and experimental data curves. Geometry, electrometer distortions, and noise effects are then studied in terms of their effects on the ideal data form. From these considerations two data reduction methods are evolved. The first is an iterative integration technique that exploits the symmetry of the experimental data about the minimum angle of attack. For the analysis of geometry effects, a second method using interval averaging was developed and studied.

SYMBOLS

Definition of terms used in this paper:

Symbol	Definition
$\hat{n}$	Experiment orifice normal
$\vec{V}_{sat}$	Satellite velocity
θ	Angle of attack
	$\arccos\left[\dfrac{\hat{n}\cdot\vec{V}_{sat}}{|\vec{V}_{sat}|}\right]$
$|\vec{V}_o|$	Most probable speed of a species of molecules with a Maxwellian distribution outside of the orifice
$|\vec{V}_i|$	Most probable speed of a species of molecules with a Maxwellian distribution inside the orifice
s	The speed ratio $= \dfrac{|\vec{V}_{sat}|\cos\theta}{|\vec{V}_o|}$
s_o	Maximum speed ratio $= \dfrac{|\vec{V}_{sat}|}{|\vec{V}_o|}$
$F(s)$	The thermal transpiration function, the idealized ratio of source to ambient density
$\eta_{s_o}(\theta)$	Correction to F(s) that accounts for the experiment chamber's geometry
$G(s)$	Geometry corrected thermal transpiration function $= F(s)\eta_{s_o}(\theta)$
ϕ	Roll angle of orifice normal
T	Satellite spin period
ω	Angular spin frequency of satellite $= 2\pi/T$
Δt	Data spacing in seconds

CONTENTS

ILLUSTRATIONS

ILLUSTRATIONS (Continued)

AN INVESTIGATION OF GEOMETRY AND NOISE CORRECTIONS TO SAN MARCO-C NEUTRAL ATMOSPHERIC COMPOSITION EXPERIMENT DATA

I. INTRODUCTION

The goal of the San Marco-C Neutral Atmospheric Composition Experiment (SM-C NACE) is the measurement of the primary constituents of the neutral atmosphere. These components are: He, O, N_2, O_2, and Ar, with provision for the measurement of contaminant gases (CO, H_2O, CO_2) having been included.

The measurement process employs a double focusing, magnetic sector type spectrometer, with which the incoming gas beam, singly ionized by electron bombardment, is separated into its component gases by their charge-to-mass ratios. These source ion currents are then converted, by means of electrometers, to voltages for telemetry. These electrometers are of a linear range switching type. Knowing the instrument transfer function allows one to convert the telemetry voltages back to source currents. These source currents combined with a knowledge of current-pressure calibrations then determine the mass spectrometer ion-source densities which are related to the ambient neutral particle densities. All of the electronic transfer functions and gas calibrations are essentially linear in nature.

In terms of geometry, the orifice normal of the enclosed ion source is in the satellite's spin equatorial plane to a good approximation ($\pm 2.0°$).

The San Marco-C satellite had a nominal orbit with initial apogee of 713 km and perigee of 213 km with a nominal spin period, T, near 8 seconds.

The ideal source density form, F(s), is shown in Figure 1 plotted vs. angle of attack. The actual data contained noise of varying severity. Figure 2 shows the spin modulated telemetry voltages for N_2 vs. time. This example was taken from strip charts of the data. Figure 3 shows the geometric relation between angle of attack and roll angle.

The theoretical relation between source and ambient densities can be deduced from elementary kinetic theory. If one assumes:

(1) Free molecular flow (mean free path >> chamber dimensions and trajectories are straight lines)

(2) Instantaneous accommodation at the orifice plane in the instrument chamber (no geometry effects)

(3) Dynamic equilibrium in the gas flows

(4) No surface reactions and/or outgassing, and,

(5) Both source and ambient particles may be described by Maxwell-Boltzmann statistics; one arrives at the equation

$$N_i^{(j)} V_i^{(j)} = N_o^{(j)} V_o^{(j)} F(s^{(j)}) \qquad (1\text{-}a)$$

where

$N_i^{(j)}$ = jth component of source density

$N_o^{(j)}$ = jth component of ambient density

$V_i^{(j)}$ = most probable speed of jth source component

$V_o^{(j)}$ = most probable speed of jth ambient component

$s^{(j)}$ = $\vec{V}_{sat} \cdot \hat{n}/|\vec{V}_o^{(j)}|$, the speed

ratio of the jth component where $\hat{n}$ is the orifice normal and $(\vec{V}_{sat} \cdot \hat{n})$ = $|V_{sat}| \cos \theta$, where θ is the angle of attack, and finally;

$$F(s) = \exp(-s^2) + s \sqrt{\pi} (1 + \operatorname{erf} s) \qquad (1\text{-}b)$$

The physical content of this equation is that since the satellite travels through the surrounding atmosphere at velocities greater than mean ambient thermal ones, the chamber orifice at small angles of attack ($|\theta| < 90°$) overtakes almost all of the gas. In contrast, at large angles ($|\theta| > 90°$) the ambient atmosphere has only a very small proportion of it's population that can overtake the satellite and hence enter the orifice.

There are two limiting cases of interest for which F(s) assumes a rather simple form. First, for s large and positive (i.e. s > 1), F(s) is well represented by the linear approximation:

$$F(s) \sim 2\sqrt{\pi} s \qquad (2)$$

Secondly, for s large and negative (i.e. s < -1):

$$F(s) \sim \exp(-s^2) \qquad (3)$$

2

and thus is exponential. Thus, for a given $s_0 = |\vec{V}_{sat}| / \vec{V}_0$, $s = s_0 \cos \theta$ and one may compute ranges of θ for which these approximations hold. Both of these cases are of interest in the analysis of atmospheric data, however, it is the linear s region that is of primary importance in density calculations. In this linear s region the ambient-source density equation (1-a) simplifies to:

$$N_i V_i = 2\sqrt{\pi} N_0 |\vec{V}_{sat}| \cos\theta \qquad (4)$$

which is independent of ambient temperature.

II. CONSIDERATIONS OF THE GEOMETRY CORRECTION TO THE THEORETICAL F(s)

If one includes geometry effects, the spin modulation of the source density is no longer adequately described by F(s) for angles of attack, θ, $< 35°$. For then, at near full ram, the directed motion of the particles becomes important. This leads to a modification of the spin modulation that may be described as:

$$G(s) = \eta_{s_0}(\theta) F(s) \qquad (5)$$

where the subscript s_0 indicates that η depends both on the angle of attack, θ, as well as the speed ratio s_0 at $\theta = 0$, where $\eta_{s_0}(\theta) > 1$. The theoretical prediction of this modification is shown in Figure 4. The dotted line visible for small θ shows the uncorrected function. It can be seen from this that for $s_0 = 10.0521$ a value characteristic of N_2 at $1150°$ K and $|\vec{V}_{sat}| = 8.3$ km/sec, the maximum effect is $\sim 40\%$ for $\theta = 0$ (full ram). The $\eta_{s_0}(\theta)$ used is that predicted by Dr. J. C. Pearl of Goddard Space Flight Center. As $\eta_{s_0}(\theta)$ is not an analytical function of θ it has been digitized from graphs and then spline interpolated for use at all angles of attack. Note that $\eta_{s_0}(\theta)$ is a monotonic decreasing function of increasing $|\theta|$.

With the inclusion of this correction the principle effect remaining is that of surface-gas interactions. These effects as predicted by Pearl results in a constant linear scaling factor to F(s) for $|\theta| > 35°$ and $\eta_{s_0} = \eta_{s_0}(\epsilon, \theta)$ for $|\theta| \leqslant 35°$, where ϵ is the recombination coefficient. For the relatively inert N_2 and the inert Ar, and He which are considered here, $\eta = \eta_{s_0}(\theta) \gtrsim 1$ and surface effects are neglected.

Thus given the geometry corrected transpiration function, G(s), one needs to consider the effects of the finite bandwidth of the electrometers through which the ion-source currents are converted to telemetry voltages. These effects will determine the shape of the theoretically observable G(s). For SM-C NACE these bandwidths ranged from 10.0 to 1.3 Hz. The satellite spin frequency was a nominal 0.125 Hz.

III. ELECTROMETER BANDWIDTH CONSIDERATIONS

To consider the electrometer effects on G(s), i.e. on the source data, one needs both a model for the electrometer and a suitable representation of G(s). G(s) was represented as a Fourier series:

$$G(s) = \sum_{N=1}^{M} a_N(s) \cos(N\theta) + b_N(s)\sin(N\theta) + a_o \qquad (6)$$

The coefficients of this series, $a_N(s)$ and $b_N(s)$ were generated by first obtaining an analytical representation of $G(s) = F(s) \, \eta_{s_o}(\theta)$ by spline interpolating $\eta_{s_o}(\theta)$. Then, the coefficients were computed from the standard integrals using a 32 point Gaussian Quadrature routine. The value of M at which the series was truncated was determined by that M which minimized:

$$\sum \left[G(s) - G_{Fourier}(s) \right]^2 \qquad (7)$$

where the sum is over all points in the spin period.

The Fourier series constructed in this manner was found to agree with the ideal G(s) to within 1% in the range $-90 \leq \theta \leq 90$ degrees.

With this G(s) representation a model electrometer was constructed from an RC circuit approximation in the form of a low pass filter. The attenuation of the Nth harmonic was then given by:

$$a'_N = \gamma_N a_N$$

$$\gamma_N = 1./\sqrt{1. + (N/Tf_2)^2} \qquad (8)$$

and the phase shift by:

$$\phi_N = \arctan(N/Tf_2) \qquad (9)$$

where f_2 is the electrometer bandwidth and T is the satellite spin period. Then,

$$G'(s) = \sum_{N=1}^{M} a'_N(s) \cos(N\theta + \phi_N) + b'_N(s) \sin(N\theta + \phi_N) + a_o \qquad (10)$$

for the post-electrometer transpiration function. The relation between the primed and unprimed coefficients is given by:

$$\begin{pmatrix} a'_N \\ b'_N \end{pmatrix} = \gamma_N \begin{pmatrix} \cos\phi_N & \sin\phi_N \\ -\sin\phi_N & \cos\phi_N \end{pmatrix} \begin{pmatrix} a_N \\ b_N \end{pmatrix} \tag{11}$$

which is easily inverted as the matrix is orthogonal, to give:

$$\begin{pmatrix} a_N \\ b_N \end{pmatrix} = \frac{1}{\gamma_N} \begin{pmatrix} \cos\phi_N & -\sin\phi_N \\ \sin\phi_N & \cos\phi_N \end{pmatrix} \begin{pmatrix} a'_N \\ b'_N \end{pmatrix} \tag{12}$$

This allows a transformation of the data to the pre-electrometer side if so desired.

The theoretically observable G'(s) that results from the transfer of this Fourier representation through the model electrometer has the following characteristics:

(1) In the region where $s > 1$, G(s) was found to be shifted, to a good approximation, by the phase shift of the fundamental harmonic with a very small attenuation. In the worst case, for a bandwidth of 1.3 Hz, and $|\theta| > 35°$ this attenuation was $\sim 0.5\%$ and the phase shift 5.49°.

(2) For $|\theta| \lesssim 35°$ the distortion of the geometry correction was more severe as the information is contained in the higher harmonics. Although the attenuation is at most 5% of the total curve amplitude for 1.3 Hz, the correction factor was attenuated by about 30%. For large bandwidths ($\gtrsim 8$ Hz) the distortion is $\sim 0.5\%$.

Figure 5 shows the pre- and post-electrometer G(s) for $s_0 = 10.052$ and a bandwidth of 1.3 Hz. The essential linearity of the electrometer transformation is shown in Figure 6. If one regards the 0.5% attenuation as negligible, the electrometer transformation in the linear s region for $|\theta| \geq 35°$ is merely shifting the roll angle axis by a constant. The transformation can thus be regarded as linear.

IV. NOISE SMOOTHING: INTEGRATION OF G(s) TO DETERMINE DENSITIES AND ROLL PHASE ANGLES

The electrometer effect has been shown to be well approximated by a linear transformation involving a change of phase in roll angle, for all bandwidths, with the restraints that $s > 1$ and $|\theta| > 35°$. The condition $s > 1$ implies $|\theta| < 75°$ for values of s_0 as small as 4, which is characteristic of He at 600° K.

5

Thus, for $35° \leq |\theta| \leq 75°$:

$$G(s) = 2\sqrt{\pi}\, s_0 \cos\theta. \tag{13}$$

From (2) and (4) the spin modulated source density is given by:

$$N_i = 2\sqrt{\pi}\, s_0 \left(\frac{N_0 |\vec{V}_{sat}|}{s_0\, V_i}\right) \cos\theta. \tag{14}$$

Setting $(N_0 V_{sat} / s_0 V_i) = 1$ for test purposes one has (13). The relation between angle of attack, θ, and roll angle $\phi = \omega t$, is given by

$$\cos\theta = a\cos\omega t - \beta \tag{15}$$

as shown in Figure 3. Also a and β are constants determined from satellite geometry and the minimum angle of attack.

It is then possible to integrate G(s) both numerically and analytically, assuming some shift, ϕ, in the roll axis:

$$I_{\pm} = \int_{\pm\phi_{35}+\delta}^{\pm\phi_{75}+\delta} G(s)\, d\phi = 2\sqrt{\pi}\, s_0 \int_{\pm\phi_{35}+\delta}^{\pm\phi_{75}+\delta} (a\cos\phi - \beta)\, d\phi \tag{16}$$

where $\pm\phi_\theta$ is determined by inverting (15). Then exploiting G(s)'s symmetry about $\phi = 0$ and using trig identities one has:

$$\frac{I_+ + I_-}{I_+ - I_-} = \frac{a\,[\cos\phi_{75} - \cos\phi_{35}]\,\sin\delta}{a\,[\sin\phi_{75} - \sin\phi_{35}]\,\cos\delta - \beta\,(\phi_{75} - \phi_{35})} \tag{17}$$

as

$$\frac{\beta\,(\phi_{75} - \phi_{35})}{a\,(\sin\phi_{75} - \sin\phi_{35})} \ll 1 \tag{17-a}$$

for SMC-NACE geometry in which the orifice normal is normal to the satellite spin axis to within $0.5°$, one has:

$$\delta = \arctan\left[\frac{\sin\phi_{75} - \sin\phi_{35}}{\cos\phi_{75} - \cos\phi_{35}}\left(\frac{I_+ + I_-}{I_+ - I_-}\right)\right] \tag{18}$$

and then:

$$s_0 = (I_+ - I_-)/\left(4\sqrt{\pi}\, a\,(\sin\phi_{75} - \sin\phi_{35})\cos\delta\right) \tag{19}$$

6

As mentioned above the s_0 determination is equivalent, within some scale factor (in this case set to unity), to determining density. Hence, density may be calculated by this method.

The shift angle, δ, determined is the combined shift resulting from the electrometer transformation plus any errors in the telemetry data.

In practice the integrals, I±, are computed using the trapezoidal rule:

$$I_+ = \frac{\omega \Delta t}{2} \left[\sum_{t_{35} \leq t_i \leq t_{75}} (G(t_i) + G(t_{i+1})) \right] \tag{20}$$

$$I_- = \frac{-\omega \Delta t}{2} \left[\sum_{-t_{35} \geq t_i \geq -t_{75}} (G(t_i) + G(t_{i-1})) \right] \tag{21}$$

where: t_i = time measured with respect to the origin ($\phi = \omega t = 0$) given by the telemetry data

Δt = data spacing (in seconds)

ω = $2\pi/T$.

Thus, it can be seen that the bulk of the calculation consists of merely summing the data points in the regions of time used.

In general, one may expect that the initial guess of the origin may be displaced far enough that the assumed conditions on s and θ are violated in the integrations. The calculated shift and density will then be only approximately correct. To compensate for this, the technique may be applied iteratively using the successive δ's to adjust the integration limits.

In testing this procedure a G(s) curve was generated with s = 10.052 and Δt = 0.001 sec, characteristic of the experiment data. This curve was then shifted 60° in roll angle and the minimum angle was set to zero to maximize the errors induced by integrating over this region. The results are shown in the table in Figure 7. The technique has converged in two iterations after the initial integration to accuracies much better than the experimental accuracies, (i.e. a residual phase error of $\sim 0.01°$ and a 0.05% error in s_0. It can be expected that in general only 1 iteration will be required as phase shifts greater than 30° should be rare.

Possible sources of systematic error in this method arise from the term $\chi = \beta \, (\phi_{75} - \phi_{35})$ in equation (17-a), i.e. the deviation of the angle between the orifice normal and the satellite spin axis from 90°. There is also an error induced by the variation in ambient density over a spin period.

In considering the orifice normal-satellite spin axis deviation, the expected deviation from the nominal value 0.5°, was used. This resulted in a zero residual phase shift (curve symmetry is preserved) and a density error of 0.37% (under estimate). It should be noted that if this deviation of density was large (e.g. a non-equatorial orifice mounting) and was known from attitude data, equation (19) can be used to correctly find the source density by including the term initially dropped from the denominator in (17).

The variation in density over a spin period is given by:

$$\exp \left(\frac{-28.0 \; V_{sat,n} \, t}{\overline{N} \; \overline{H}} \right) \tag{22}$$

where: t is the time in seconds measured from the spin period's center, $\overline{H}$, $\overline{N}$ are the mean density scale height and the mean molecular weight, 28 is the molecular weight of N_2, $V_{sat,n}$ is the vertical satellite speed. Using the nominal SM-C orbit the exponential effect was maximized by using:

$$V_{sat,n} \quad = \; 0.3 \, km/sec$$
$$\overline{H} \qquad = \; 37.86 \, km$$
$$\overline{N} \qquad = \; 11.79$$

Where $\overline{H}$ and $\overline{N}$ are taken from the 1971 Jacchia model thermosphere for a 400 km altitude and an exospheric temperature of 600°K. Using the nominal satellite period one has:

$$\exp \, (- \, 0.0188 \, t), \; - 4 < t < 4 \; sec.$$

This effect was found to result in a residual error in phase angle of 0.85 degrees with s_0 accurate to 0.05%. The effect of this altitudinal density variation is to give a cosine fit of the same amplitude but phase shifted, with respect to a constant density fit.

In conclusion, this method allows the rapid determination of both roll phase angle and source density to a high degree of accuracy. The density determination is performed using a sample of about 50% of the data points in the angle of attack range -90 to 90 degrees and also implicitly averages the noise over very long intervals. As it provides a density characteristic of a spin period it's only

deviation results from the ambient density variation over a cycle. Since the exponent is small the variation is approximately linear:

$$\exp(-0.0188\,t) \sim 1.0 - 0.0188\,t$$

the assignment of the density to the midpoint of the spin period thus gives the true density at the midpoint with errors of order $(0.0188\,t)^2$. In Figure 8, G(s) and a cosine density fit are shown.

One additional error source for density determinations is that due to the uncertainty in minimum angle of attack, θ min, of approximately ± 2 or 3 degrees. This error enters through the $\cos(\theta min)$ dependence of a in equation (19). For example, for θ min $= 20°$ a deviation of $\pm 2\%$ may be expected. This is apparently the largest error contribution of the three that were investigated and thus sets an upper limit on the accuracy that may be achieved.

V. NOISE SMOOTHING: INTERVAL AVERAGING

A second method of spin modulated density determination considered was interval averaging. In this technique a simple average:

$$\overline{G(\bar{t})} = \frac{1}{N} \Sigma\ G_i(t) \tag{23}$$

is taken over some odd number of points with the average being assigned to the interval's midpoint, $\bar{t}$. This process is also known as taking a "running mean" of a curve. If the roll angle phase is determined as in Section IV, then it can be shown that this method may be used to average out noise which yields source densities upon division by the spin modulation factor.

It was desired to find the interval size that would both smooth the data best while simultaneously least distorting it. This goal resulted in an investigation of the following considerations for the choice of an interval size, δt:

(1) The error induced by the averaging processing itself,

(2) The degree of noise smoothing obtained, and;

(3) The amount by which the geometry correction factor is "washed out".

A computer analysis was made of the variation of fractional error, f as a function of angle of attack, where:

$$f = \left(\overline{G(\bar{t})} - G(\bar{t})\right) / G(\bar{t}) \tag{24}$$

The results, as shown in Figure 9 for an interval size of 0.1 seconds and data sampling rate of 0.01 seconds, were that:

(1) In the linear s region f was constant, for η_{s_o} $(\theta) \sim 1$, quite small and negative,

(2) For η_{s_o} $(\theta) > 1$ f showed a characteristic oscillatory structure significantly greater than in (1) but still small,

(3) In the exponential s region the error is exponentially increasing and positive.

Thus, f essentially measures the deviation of G(s) from linearity in s. In the exponential s region there exists a systematic error in that the linear average of an exponential function will always be greater than the function evaluated at the interval's midpoint whenever the function is monotonically increasing or decreasing over the interval.

As it is only the linear s region that is of interest in density determination, and as it is only here that the averaging process does not contain the aforementioned systematic error, only for this region will a quantative relation between f and δt be derived.

If one now considers a Taylor series expansion of f about the interval's midpoint for

$$G(t) = 2\sqrt{\pi} \, s_o a \cos\omega \, (\bar{t} + t_i) \tag{25}$$

by symmetry, odd powers of ωt will cancel when summed over the interval and;

$$f_{\Delta t} = \frac{-\omega^2}{2N} \sum_{-\delta t/2 \,\leqslant\, t_i \,\leqslant\, \delta t/2} t_i^2 \tag{26}$$

where:

ω = satellite spin frequency (rad/sec)

N = number of points in averaging interval

δt = averaging interval size

t_i = time of the ith data point measured from the interval's center (sec)

Δt = data point spacing in seconds.

Note that this result is independent of s. Figure 10 compares the values of f with those calculated by computer. The result of neglecting the remaining terms of order $(\omega t_i)^4$ is an error in the predicted f of $\sim 10^{-4}$.

As can be seen in the table of Figure 10, the formula is of high precision. This formula can therefore be used to estimate the effects of data compression, i.e. not averaging every point but selecting out some subset. For example, suppose 1 out of every 10 data points was chosen for averaging then the increase in error is given by the ratio $f_{.01}/f_{.001}$, as a function of averaging interval size which can be calculated. The result of this calculation is shown in Figure 11. As the error increase is small, preliminary selection may be desired to minimize computation time.

Consider the final case of $\eta_{s_0}(\theta) > 1$ for small angles of attack. Retaining the linear and cubic terms in the expansion, one has:

$$f_{\Delta t} = \left\{ \frac{1}{N\eta_{s_0}(\omega\bar{t})} \sum \eta_{s_0}(\omega(\bar{t}+t_i)) \left[1.0 - (\tan\omega\bar{t})\,\omega t_i \right. \right.$$
$$\left. \left. - (\omega t_i)^2/2 + (\tan\omega\bar{t})(\omega t_i)^3/6 \right] \right\} - 1.$$

(27)

where:

$$-\frac{\delta t}{2} \leqslant t_i \leqslant \frac{\delta t}{2}$$

Note that f now depends on both s_0 and roll angle. In Figure 12, $f_{.01}$ and $f_{.001}$ are plotted vs. angle of attack for $\delta t = 0.1$ sec. For $f_{.01}$ the result agreed with the computer calculation in Figure 9 to within 1%. It is also notable that the increase of f with increasing Δt (data selection) is small.

Figure 12 also demonstrates the "washing out" effects in the smoothing down of the G(s) peak (See Figure 4) and the enhancement of the lower sides of the correction as it is smeared out more uniformly by the averaging process.

In summary, from a consideration of systematic averaging errors, the most severe is that produced by the "washing out" of the geometry correction if this is to be studied.

In the actual noise smoothing itself, it is reasonable to ask what is the best interval size in terms of minimizing the noise contribution to the source density. As shown in Figure 2, it would appear that by inspection most of the noise amplitude is contained in the higher harmonics. Given this fact, consider the amplitude of the Nth noise harmonic, H_N of a Fourier series representing the post-electrometer noise.

11

Where: $G(s)_{\text{with noise}} = G(s)_{\text{ideal}} + H(s)_{\text{noise}}$,

Then $H_N = a_N \cdot \cos(\omega t + \phi_N)$, and for a fixed averaging interval size, δt, the greatest error magnitude contribution to the mean is:

$$\frac{a_N \int_{\text{half cycle}} \cos(\omega t + \phi_N)}{\delta t} \qquad (28)$$

Where: a_N is the constant coefficient of the Nth harmonic, and,
ϕ_N is the phase angle of the Nth harmonic.

Thus, the contribution is minimized by making δt as large as possible.

In conclusion, for interval averaging as a method of minimizing noise contributions to source densities, there are two separate regions of interest:

(1)   For $\eta_{s_0}(\theta) \sim 1$ ($|\theta| \gtrsim 35°$) the only restraint is on the magnitude of f. This should allow interval sizes as large as 0.5 sec with systematic errors of $<1\%$.

(2)   For $\eta_{s_0}(\theta) > 1$, ($|\theta| \lesssim 35°$) and electrometer bandwidths $> 8\,\text{Hz}$, the most important limitation on interval size is the geometry correction being "washed out". This appears to set an upper limit of approximately 0.1 sec.

CONCLUSION

The electrometer transformation has been studied and found to be well approximated by linear transformation in which only the roll angle is shifted for angles of attack θ, such that $75 \geqslant |\theta| \geqslant 35$ degrees. This also applies for $|\theta| \leqslant 35$ degrees when the electrometer bandwidth is $\geqslant 8\,\text{Hz}$. For small bandwidths (e.g. $1.3\,\text{Hz}$) the transformation is non-linear for $|\theta| \leqslant 35°$ and must be treated separately.

Exploiting the fact that the essential cosine curve representing G(s) for $35 \leqslant |\theta| \leqslant 75$ degrees when passed through the SM-C NACE electrometers is preserved, an iterative integration scheme was developed to fit G(s) with a cosine curve. This method rapidly and accurately determines the roll angle phase and a representative source density for the spin period. This scheme also implicitly greatly dampens noise contributions to density for reasons given in section V, as the averaging intervals (i.e. the intervals of integration) are on the order of 0.8 sec.

12

Finally, interval averaging was studied as a possible means of examining the geometry correction effect for large bandwidth electrometers ($\gtrsim 8$ Hz). The restraint here was primarily the washing out of detail that limited the interval size to ~ 0.1 sec for the SM-C nominal spin period of 8 sec.

ACKNOWLEDGEMENTS

REFERENCES

1. San Marco-C Satellite Payload Description Document, Centro Ricerche Aerospaziali, Rome, Oct. 1970.

2. Application of the Green's Function to the Analysis of Internal Flows of Rarified Gases, John C. Pearl, Uriel Vogel.

3. SM-C Geometry Corrections to F(s), J. C. Pearl, 2/27/70, Memorandum.

4. Fourier Series, Tolstov, Prentice-Hall Inc., 1962, pp. 123-125.

5. Electronics for Scientists, Howard V. Malmstadt, 1963, W. A. Benjamin & Co.

6. A Critical Survey of Upper-Atmosphere Density Measurements by Means of Ionization Gauges, M. P. Friedmann, July 15, 1966, SAO Special Report #217.

7. The Thermal Transpiration Equation: Tables of F(s) vs. s, Y. S. Hsu, University of Michigan, Scientific Report MS-2.

8. Spline Interpolation on a Digital Computer, R. Thompson, X-692-70-261, July 1970.

9. Revised Static Models of the Thermosphere and Exosphere with Empirical Temperature Profiles, L. G. Jacchia, May 5, 1971, SAO Special Report #332.
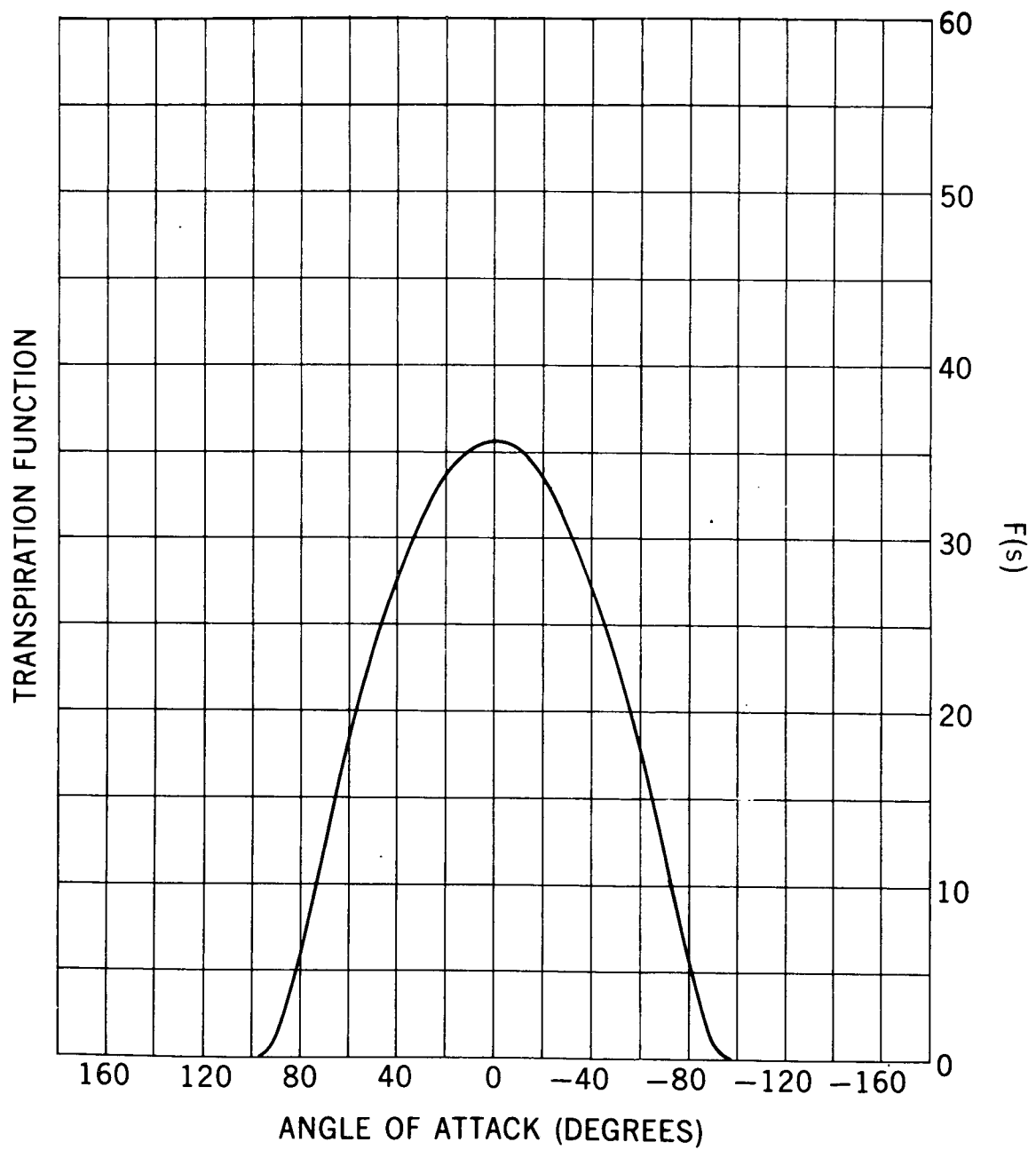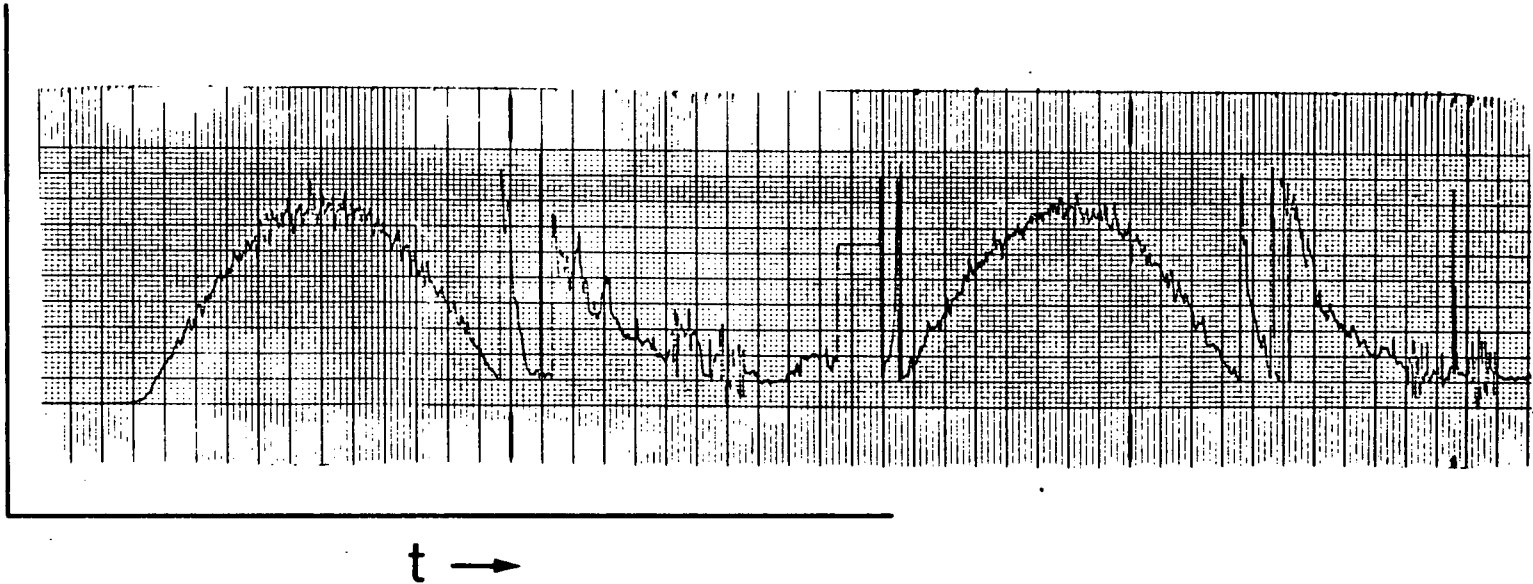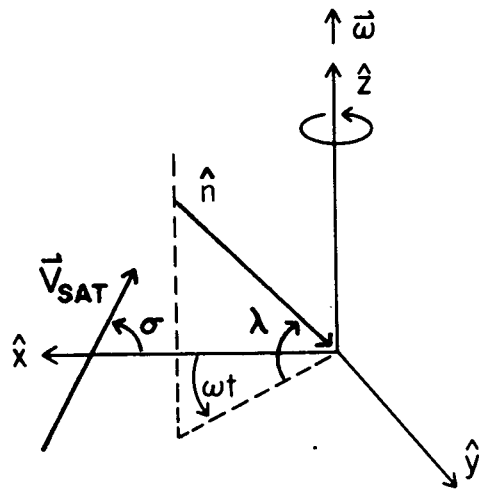
Figure 1. F (s) (No Geometry Correction)

Figure 2. San Marco-C NACE Data Channel 7, Molecular Nitrogen Showing Noise Structure

$\vec{V}_{SAT}$ = SATELLITE VELOCITY

$\hat{n}$ = ORIFICE NORMAL

θ_{min} = MINIMUM ANGLE OF ATTACK

$\hat{z}$ = SATELLITE SPIN AXIS

V_{mp_0} = MOST PROBABLE MOLECULAR VELOCITY

o = OUTSIDE OF ORIFICE, i = INSIDE

$s = \vec{V}_{SAT} \cdot \hat{n} / V_{mp_0}, \ V_{mp_0} = \sqrt{\dfrac{2KT_0}{m}}$

$s = s_0 (\alpha \cos \omega t - \beta), \ s_0 = V_{SAT} / V_{mp_0}$

$\alpha = \cos \sigma \cos \lambda = CONSTANT, \ \beta = \sin \sigma \sin \lambda = CONSTANT$

$\sigma + \lambda = \theta_{min}$

TRANSPIRATION EQUATION: $N_i V_{mp_i} = N_0 V_{mp_0} F(s)$

Figure 3. Satellite Geometry
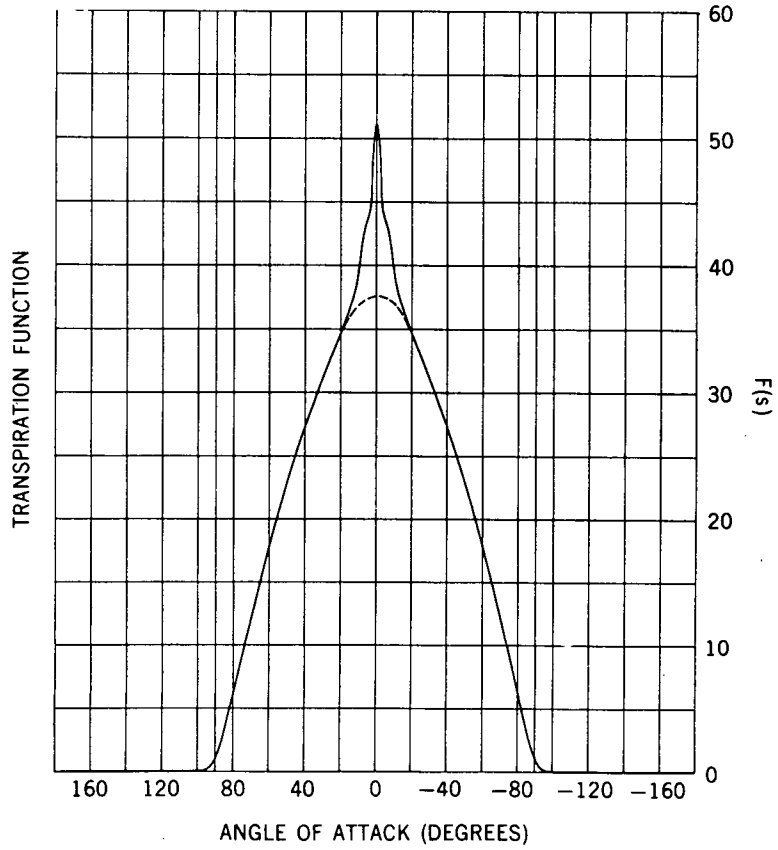
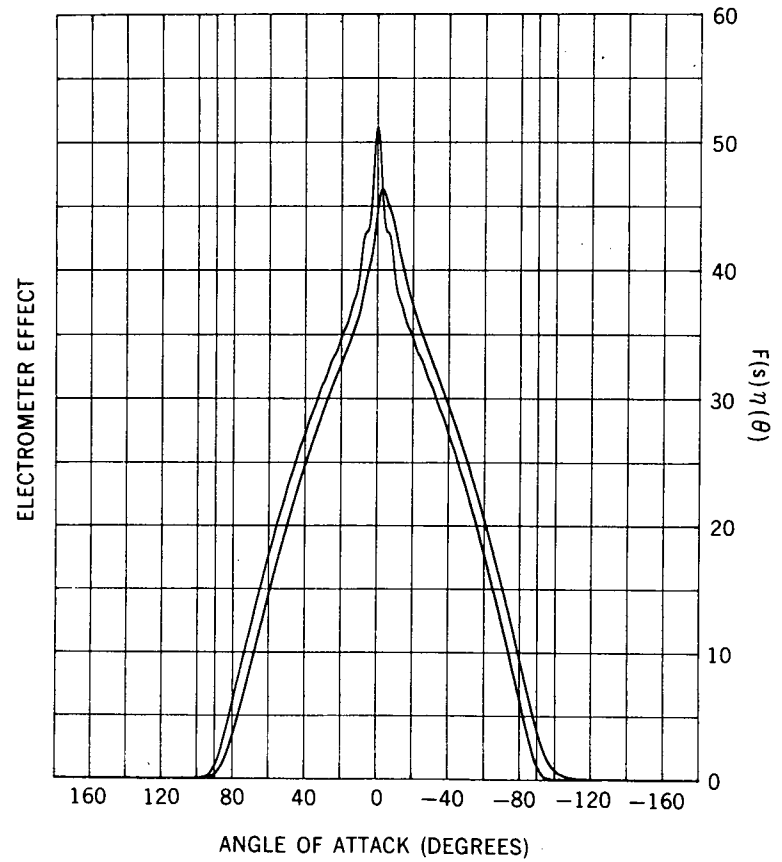Figure 4. $G(s) = F(s) \eta(\theta)$ Geometry Effect Included

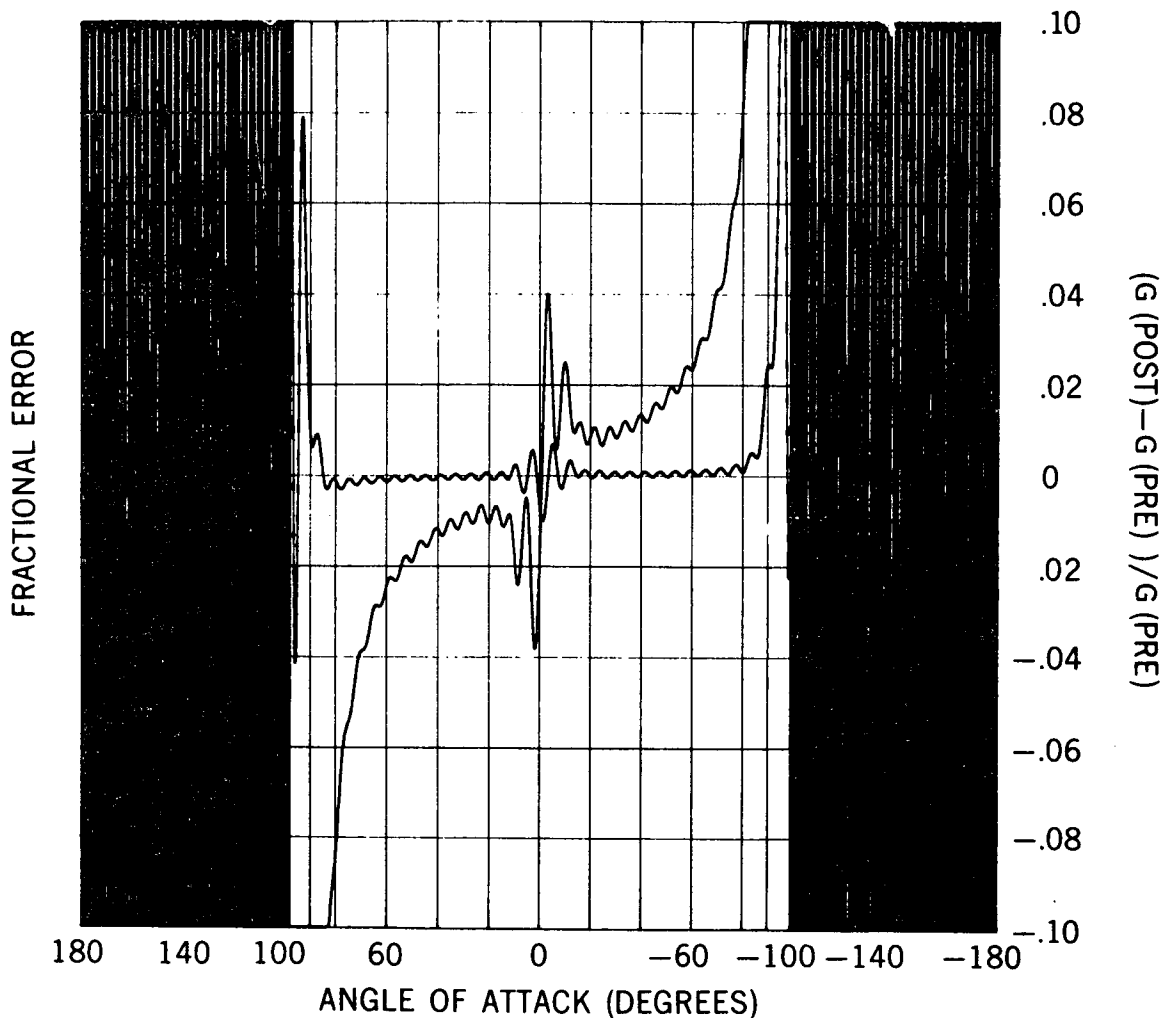Figure 5. Effect of $G(s)$ Passage through a Model 1.3 Hz Electrometer

17

Figure 6. Effect of Shifting G (s), Post Electrometer, by Phase Shift in Fundamental Harmonic

Iteration #	$\delta_{SHIFT}^{(i)}$	$-\delta_{TOTAL}^{(i)}$	$\delta_{ERROR}^{(i)}$	$s_o^{(i)}$	$(s_o^{(i)} - s_o) / s_o$
0	-34.9801°	34.9801°	25.0199°	12.3838	.231974
1	-23.9264	58.9065	1.0935	10.4299	.037594
2	- 1.0821	59.9886	.0114	10.0576	.000557
3	- 1.26 x 10⁻⁵	59.9886	.0114	10.0573	.000527
4	- 1.26 x 10⁻⁵	59.9886	.0114	10.0573	.000527

Figure 7. Sample of Integration Results using Theoretical G (s) $s_o = 10.0520$, $\lambda = 0$, $\theta_{min} = 0$, $\delta_{shift} = 60°$
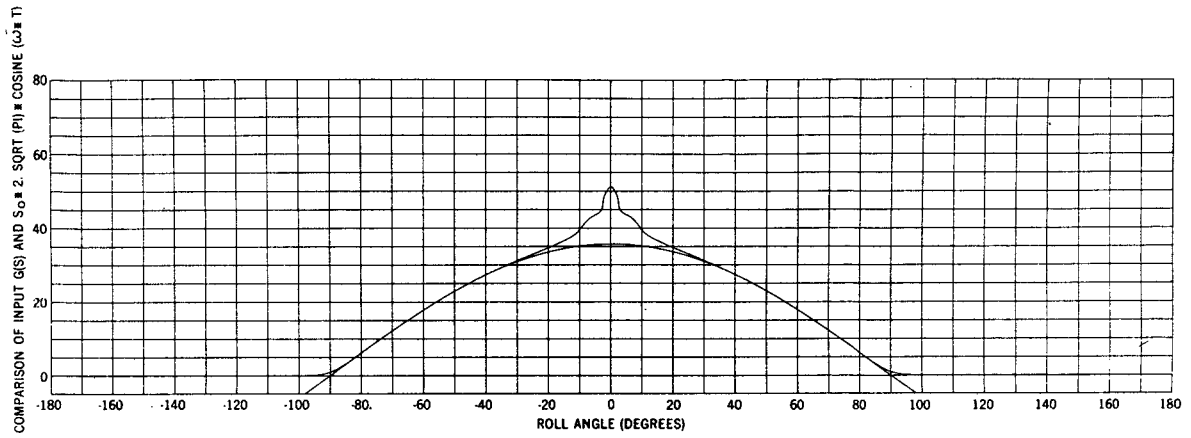
18

Figure 8. Density Determination and Phase Shift Calculation

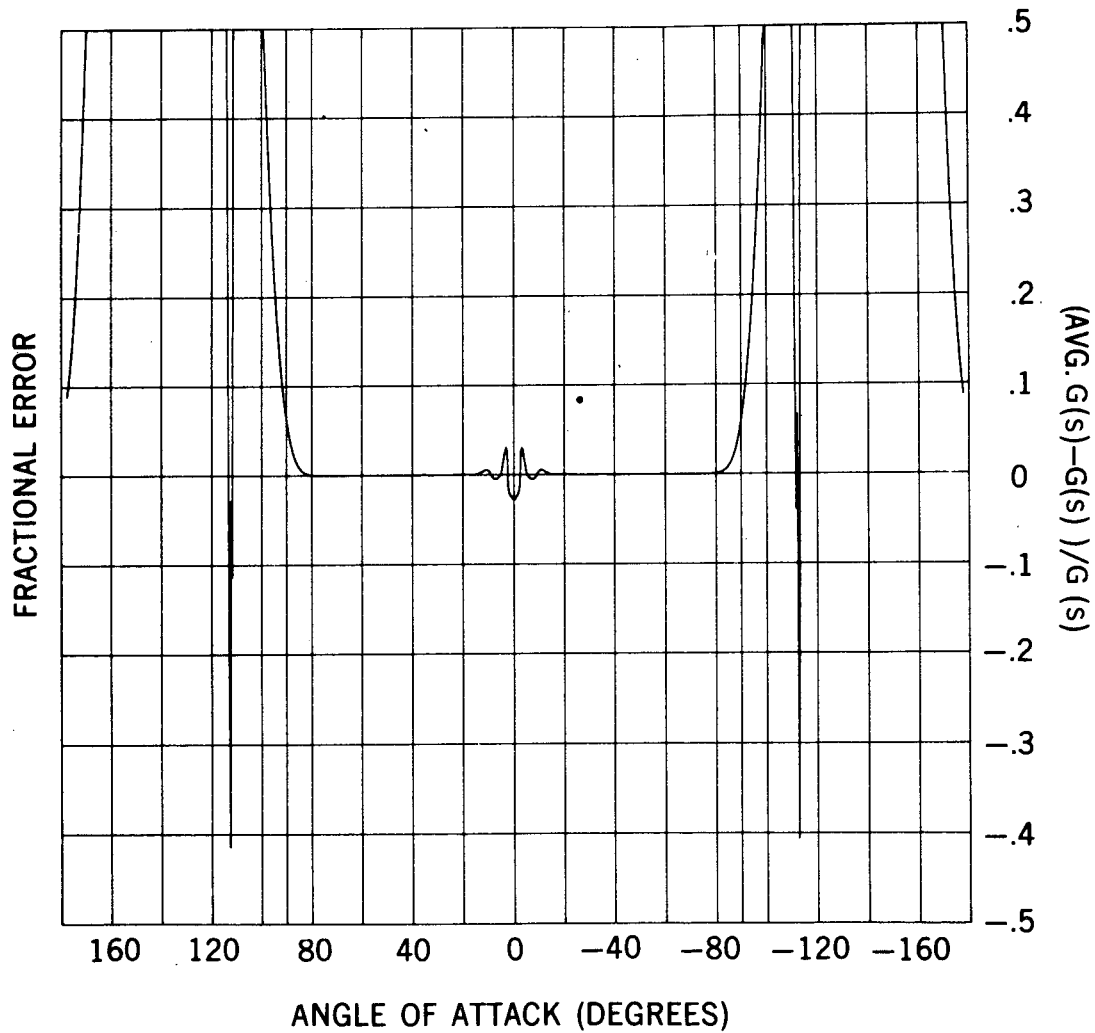Figure 9. Fractional Error vs. Angle of Attack

19

δt (m sec)	f predict	f compute	$\dfrac{(\text{f predict} - \text{f compute})}{\text{f compute}}$
40	-6.168×10^{-5}	-6.20×10^{-5}	-.0051
60	-1.233×10^{-4}	-1.23×10^{-4}	.0024
80	-2.056×10^{-4}	-2.06×10^{-4}	-.0032
100	-3.07×10^{-4}	-3.08×10^{-4}	-.0034
140	-5.757×10^{-4}	-5.78×10^{-4}	-.0040
200	-1.131×10^{-3}	-1.133×10^{-3}	.0015

Figure 10. Comparison of Computed and Predicted values of f for Region I

$|\theta| \geq 35°$
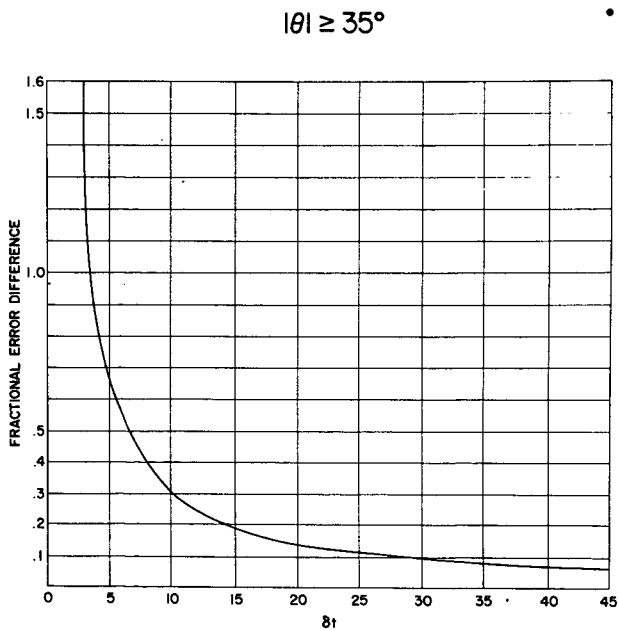
Figure 11. The Effect of Sampling on Fractional Error
for Interval Averaging
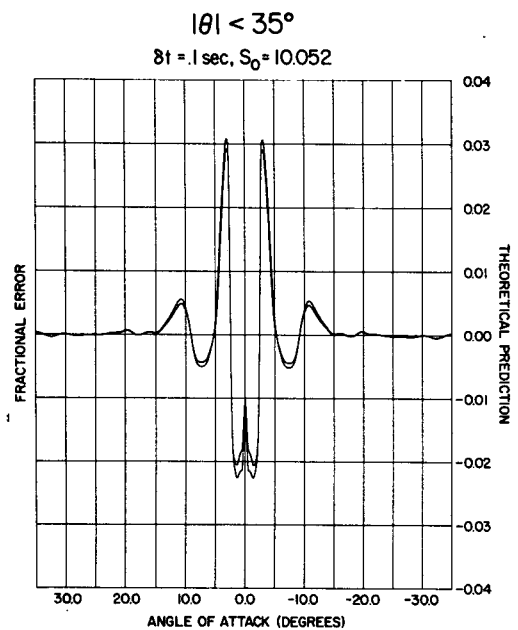
$|\theta| < 35°$

$\delta t = .1$ sec, $S_0 = 10.052$

Figure 12. The Effect of Sampling on
Fractional Error for Interval Averaging